

Highly reversible and long-lived zinc anode assisted by polymer-based hydrophilic coating

Hang Chen, Xinghan Yuan, Hongmei Qin, and Chuanxi Xiong (✉)

School of Materials Science and Engineering, Wuhan University of Technology, Wuhan 430070, China

© Higher Education Press 2023

ABSTRACT: Rechargeable aqueous zinc-ion batteries (AZIBs) are the most promising candidates for the energy storage due to their high safety, rich resources, and large specific capacity. However, AZIBs using neutral or slightly acidic electrolytes still face side effects and zinc dendrites on the anode surface. To stabilize the Zn anode, a chemically stable and multi-functional coating of polyvinylidene fluoride (PVDF) and 4,4'-(hexafluoroisopropylidene)diphthalic anhydride (6FDA) was prepared on the Zn surface. The anhydride groups in 6FDA can improve the hydrophilicity, promoting the migration of zinc ions. Besides, PVDF is compatible with 6FDA because of the presence of organic F-containing groups, which can also effectively reduce the nucleation overpotential and exhibit the dendrite-free Zn deposition/stripping. The PVDF/6FDA@Zn symmetric cell can cycle for 5000 h at a current density of $0.5 \text{ mA}\cdot\text{cm}^{-2}$, maintaining the extremely low polarization voltage and overpotential of 28 and 8 mV, respectively. The PVDF/6FDA@Zn||MnO₂ full cell can remain a specific capacity of $\sim 90 \text{ mAh}\cdot\text{g}^{-1}$ after 2000 cycles at $1.5 \text{ A}\cdot\text{g}^{-1}$. This simple method achieves a reversible Zn anode, providing an inspiring strategy for ultra-long-cycle AZIBs.

KEYWORDS: aqueous zinc ion battery; zinc anode; polyvinylidene fluoride; composite film

Contents

- 1 Introduction
- 2 Experimental
 - 2.1 Materials
 - 2.2 Preparation of PVDF/6FDA@Zn anode
 - 2.3 Preparation of α -MnO₂ cathode
 - 2.4 Fabrication of coin batteries
 - 2.5 Characterization
- 3 Results and discussion
- 4 Conclusion

Declaration of competing interests

Received July 23, 2023; accepted October 22, 2023

E-mail: cxiong@whut.edu.cn

Acknowledgements

Electronic supplementary information

References

1 Introduction

Lithium-ion batteries (LIBs) are dominant in the field of electrochemical energy storage because of the incomparable advantages of high energy density and power density [1–2]. However, growing concerns about costs, safety, pollution, and resource constraints of LIBs have prompted the search for alternative energy storage technologies [3–5]. Zinc-ion batteries (ZIBs) are considered the most promising commercial alternatives to

expensive or dangerous LIBs. Zinc-based batteries, containing metal elements that possess multi-electron transfer properties, have high theoretical capacities ($5849 \text{ mAh}\cdot\text{cm}^{-3}$ and $820 \text{ mAh}\cdot\text{g}^{-1}$). In addition, a redox potential as low as -0.76 V (vs. the standard hydrogen electrode (SHE)) prevents the violent reaction between Zn metal and water [6–7]. Furthermore, the aqueous solution has a much higher ionic conductivity (about $10\text{--}150 \text{ mS}\cdot\text{cm}^{-1}$) than that of the organic electrolyte (about $1\text{--}10 \text{ mS}\cdot\text{cm}^{-1}$), which endows rechargeable aqueous zinc-ion batteries (AZIBs) with better rate performance [8]. Unlike other emerging batteries that use organic electrolytes, zinc metal can be directly used as the anode for AZIBs. This feature has recently become very attractive, especially due to its safety, non-flammability, low cost, and high power. Meanwhile, AZIBs combine supercapacitors and conventional battery devices, achieving an acceptable balance between power density and energy density [9].

So far, the development of AZIBs is still in its early stages, and various issues that arise during the AZIBs cycling impact the feasibility of scale-up production. The fatal weakness of the zinc metal anode is its thermodynamic instability in the water electrolyte, which triggers hydrogen evolution reaction (HER) and dendrite formation followed by corrosion reaction processes [10]. In practice, the reduction of zinc does not produce a uniform and smooth plane, signifying that the newly formed reduced zinc does not always grow horizontally, but rather shows preferential orientation [11–13]. This preferential growth orientation produces many heterogeneous zinc and exacerbates the uneven distribution of ion flux due to self-amplification behaviors, resulting in uncontrolled dendrites like the LIBs system [14–15].

To address the challenges, there are three common optimization methods about the Zn anode in AZIBs, which are host structural design, electrolyte optimization, and surface modification [16–18]. Structural design is often adopted in electrode protection because of its significant advantage of prolonging the cycle and decreasing the overpotential, including the Au coating layer (Au–Zn) [19] and the three-dimensional (3D) nanoporous Zn anode [20]. These structural designs mainly focus on the direct design of the zinc metal anode host or covering the surface of the zinc metal anode with a layer of a metal that is compatible with zinc. However, the problem with using these methods to design the main

structure is the replication of manufacturing processes and the associated high costs. Advanced electrolyte solution additives have also been proven to positively impact the stability of zinc anodes. These additives include polyacrylamide (PAM), sodium dodecyl sulfate (SDS), hexadecyl trimethyl ammonium bromide (CTAB), triethyl phosphate (TEP), polyethylene glycol (PEG), and thiourea (TU) [21–23]. In addition, the use of high concentrations of zinc di[bis(trifluoromethylsulfonyl)imide] ($\text{Zn}(\text{TFSI})_2$) and zinc trifluoromethanesulfonate ($\text{Zn}(\text{TfO})_2$) electrolytes has also driven the development of AZIBs [24–27]. However, the high cost of salts containing TFSI and TfO poses a challenge to practical application, and they are also harmful, which goes against the commitment to “green chemistry” of AZIBs.

In contrast, the surface modification of zinc metal anodes is a simple, effective, and low-cost method, particularly in the construction of solid electrolyte interfaces (SEIs) using flexible polymer materials on the anode surface. For example, Chen et al. [28] dropped a solution of polyacrylonitrile (PAN) containing $\text{Zn}(\text{TfO})_2$ onto the surface of zinc metal to obtain a PANZ coating. The addition of $\text{Zn}(\text{TfO})_2$ improved the hydrophilicity of the PAN coating and significantly reduced the interface resistance of the zinc anode. As a result, the symmetric cell exhibited stable cycling for over 1140 h. Inspired by the principle of bioadhesion, Zeng et al. [29] constructed the stable SEI of polydopamine (PDA) by *in situ* electrochemical polymerization of dopamine additive, which provided multifunctional features such as excellent hydrophilicity, adjustable Zn nucleation deposition, rapid Zn^{2+} transport, and strong adhesion ability. Niu et al. [30] proposed a hydrophilic adhesive coating (HAC) composed of polyacrylamide-*co*-polymethyl acrylate copolymer (PAMMA) as an artificial interface for SEI to alleviate the dendrite growth and side reactions. By controlling the mass ratio of hydrophilic acrylamide to hydrophobic methyl acrylate, the optimal balance between hydrophilicity and adhesion could be achieved. Moreover, PAMMA polymers contained abundant carbonyl groups in both monomer units, which could serve as ion plating/stripping sites. Hieu et al. [31] used the spin-coating method to prepare a thin and highly polar layer of β -phase poly(vinylidene difluoride) (β -PVDF) coated onto the zinc anode. The β -PVDF layer had good elasticity and stability, which could effectively optimize the zinc plating process and inhibit the corrosion. Therefore, based on the effective inhibition of the dendritic growth of zinc metal

anodes by flexible and hydrophilic polymer coatings, we propose a method to enhance the hydrophilicity of PVDF, which can be achieved by the utilization of small-molecule organic compounds containing anhydride groups. The objective is to achieve stable zinc plating/stripping and enhance the cycle life of AZIBs [32–34].

In this work, a polymer interphase consisting of PVDF and 4,4'-(hexafluoroisopropylidene)diphthalic anhydride (6FDA) is applied to the surface of the zinc anode by a facile spin coating method. The hydrophilicity and fluorine-containing functional groups of PVDF/6FDA can attract zinc ions in the electrolyte and fulfill the desolvation of $[\text{Zn}(\text{H}_2\text{O})_6]^{2+}$ to provide an uniform diffusion path on the surface, which contributes to the flat Zn depositing/stripping [35–37]. Moreover, the PVDF/6FDA layer has sufficient flexibility and low creep properties, capable of resisting volume changes during the cycle. Consequently, PVDF/6FDA@Zn symmetric cells could cycle for 5000 h with a low polarization voltage of 28 mV at $0.5 \text{ mA}\cdot\text{cm}^{-2}$, and the full cell shows excellent cycling stability with a specific capacity of $90 \text{ mAh}\cdot\text{g}^{-1}$ at $1.5 \text{ A}\cdot\text{g}^{-1}$ over 2000 cycles. Therefore, it is seen that PVDF/6FDA coatings based on flexible polymers have following advantages: (i) PVDF is inexpensive and readily available; (ii) the PVDF/6FDA coating exhibits good flexibility and can accommodate to volume changes caused by the zinc plating/stripping process; (iii) compared to PVDF coatings, the hydrophilic properties of PVDF/6FDA can effectively reduce the interface impedance, which is more conducive to the rapid migration of zinc ions.

2 Experimental

2.1 Materials

PVDF was purchased from Solvay (PVDF 6010). 6FDA was purchased from Aladdin (99%). N,N-dimethylformamide (DMF; 99.8%) used as the solvent was obtained from Sinopharm Chemical Reagent Co., Ltd. (Shanghai, China). The deionized water used was self-made in the laboratory. Concentrated sulfuric acid, manganese sulfate monohydrate ($\text{MnSO}_4\cdot\text{H}_2\text{O}$) and potassium permanganate (KMnO_4) used in the synthesis of manganese dioxide were purchased from Sigma-Aldrich (Shanghai, China). N-methylpyrrolidone (NMP)

was used as a dispersant purchased from Aladdin. Zinc foil with a thickness of 0.1 mm was used as the anode. Copper foil with a thickness of 0.03 mm was used as the cathode of the half-cell. High-purity titanium foil with a thickness of 0.03 mm was used as the fluid collector. Glass fiber (Whatman GF/D 1823) was as the separator for CR2016 coin cells.

2.2 Preparation of PVDF/6FDA@Zn anode

1 g PVDF and 0.3 g 6FDA were added into 5 g DMF with stirring to obtain a homogeneous solution. The PVDF/6FDA film was then coated on the Zn foil surface using the spin-coating method at a spin-speed of $2000 \text{ r}\cdot\text{min}^{-1}$ for 1 min.

2.3 Preparation of α - MnO_2 cathode

At first, 2 mL of $0.5 \text{ mol}\cdot\text{L}^{-1} \text{ H}_2\text{SO}_4$ and 0.507 g $\text{MnSO}_4\cdot\text{H}_2\text{O}$ were added into 90 mL deionized water. Then 20 mL of $0.1 \text{ mol}\cdot\text{L}^{-1} \text{ KMnO}_4$ solution was slowly added and stirred for 2 h. Subsequently, the product was obtained by the hydrothermal reaction for 12 h at $120 \text{ }^\circ\text{C}$. Finally, it was washed, filtered and dried at $80 \text{ }^\circ\text{C}$ to obtain α - MnO_2 . α - MnO_2 (70 wt.%), conductive carbon black (20 wt.%) and PVDF binder (10 wt.%) were mixed into NMP, and then coated on Ti foil. The α - MnO_2 cathode was thus obtained after drying at $80 \text{ }^\circ\text{C}$ for 24 h.

2.4 Fabrication of coin batteries

The Zn anode and the α - MnO_2 cathode were punched into disks ($D = 10 \text{ mm}$). $\text{Zn}||\text{MnO}_2$ was assembled by pairing the zinc anode with the cathode using glass fiber ($D = 19 \text{ mm}$) and $2 \text{ mol}\cdot\text{L}^{-1} \text{ ZnSO}_4 + 0.2 \text{ mol}\cdot\text{L}^{-1} \text{ MnSO}_4$ aqueous solution as the separator and the electrolyte, respectively. For the assembly of $\text{Zn}||\text{Zn}$ symmetric cell and $\text{Zn}||\text{Cu}$ batteries, $2 \text{ mol}\cdot\text{L}^{-1} \text{ ZnSO}_4$ aqueous solution was used as the electrolyte.

2.5 Characterization

The ion conductivity of PVDF/6FDA coatings was measured using the following method. The PVDF/6FDA film was wetted with the electrolyte before placement in a stainless steel foil. Then the electrochemical impedance spectroscopy (EIS) was performed at 10 mV with the frequency ranging from 0.01 Hz to 100 kHz to research the symmetric cell. The ionic conductivity (σ) can be

obtained with the following equation:

$$\sigma = \frac{L}{RS} \quad (1)$$

where L (mm) is the thickness of the polymer coating, R (Ω) is the impedance of the film, and S (mm^2) is the contact area between the polymer-based coating and the stainless-steel foil.

The morphologies of the PVDF/6FDA@Zn foil before and after electrodeposition were observed by field emission scanning electron microscopy (FESEM; Hitachi S-4800), along with energy dispersive X-ray spectroscopy (EDS) mapping. The crystalline structures of the bare Zn electrode and the PVDF/6FDA@Zn electrode were investigated by X-ray diffraction (XRD) with the Cu $K\alpha$ radiation at a scan rate of $1^\circ \cdot \text{min}^{-1}$. Contact angles of different electrodes were measured by Biolin contact angle measuring instrument.

Galvanostatic charge/discharge (GCD) measurements were conducted using the LAND test system. Cyclic voltammetry (CV) and EIS were performed on an electrochemical workstation (CHI660E). The CV was used to investigate the reversibility of electrochemical reactions. The full cells were tested at a scan rate of $1 \text{ mV} \cdot \text{s}^{-1}$ in the potential range of 0.6–1.8 V. The EIS spectra of symmetric cells were obtained under the potentiostatic EIS mode condition with the amplitude of 10 mV and a frequency range of 0.01 Hz to 100 kHz. A three-electrode system was used for the polarization measurement with zinc metal as the working electrode, a Pt electrode as the counter electrode, a saturated calomel electrode as the reference electrode, and $2 \text{ mol} \cdot \text{L}^{-1}$ ZnSO_4 solution as the electrolyte.

3 Results and discussion

As we know, the fatal weakness of the bare zinc anode is the thermodynamic instability in aqueous electrolytes, which triggers HER followed by the corrosion and dendrite formation [38]. Thus, based on the principle of surface modification protection using a spin coater for polymer materials, it would be highly promising to create an interphase that isolates water molecules but allows for the transmission of ions between the electrolyte and Zn [39–40]. In this work, PVDF is dissolved in DMF, and the PVDF coating is prepared on the surface of the zinc foil (PVDF@Zn) through the rotary coating process.

Similarly, 6FDA is uniformly dispersed in the PVDF polymer solution, and the PVDF/6FDA protective film is coated onto the surface of zinc metal using a spin coating process (PVDF/6FDA@Zn). The chemical structure of 6FDA is shown in Fig. S1, and the schematic diagram of the working principle of the PVDF/6FDA protective layer is shown in Fig. 1. During the charging and discharging process of AZIBs, if no measures are taken to protect the zinc metal negative electrode, dendrites will form on the bare zinc surface after multiple charging and discharging cycles. The local current density of dendrites increases, making zinc ions more inclined to be deposited in the dendrite area. As time goes by, dendrites gradually grow, reaching a critical point and piercing the separator, causing a short circuit in the battery. On the contrary, under the action of the PVDF/6FDA ultra-thin coating, zinc ions are deposited parallel to the substrate. The principle of orderly deposition of zinc ions onto the surface of zinc metal is due to the electrostatic attraction between polar functional groups ($-F$) in the PVDF polymer coating and zinc ions. At the interface between the solid electrolyte solution, polar functional groups can effectively promote the desolvations of zinc ions in the electrolyte solution, guiding the orderly deposition of zinc ions onto the surface of zinc metal. In addition, the coating also inhibits the growth of dendrites to some extent through physical actions.

As shown by Fourier transform infrared spectroscopy (FTIR) results in Fig. 2(a), the PVDF/6FDA film has characteristic peaks at 1785 and 721 cm^{-1} , corresponding to $\text{C}=\text{O}$ and $\text{C}-\text{F}$ stretching vibrations in 6FDA, respectively. Besides, it also has characteristic peaks of β -PVDF at 510 and 840 cm^{-1} . SEM images (Figs. 2(b) and 2(c)) along with EDS mapping images (Figs. 2(d)–2(f)) show that PVDF and 6FDA have great compatibility, and it is notable that the O element originating from 6FDA is evenly distributed in the PVDF/6FDA coating. This proves that the PVDF/6FDA coating has been

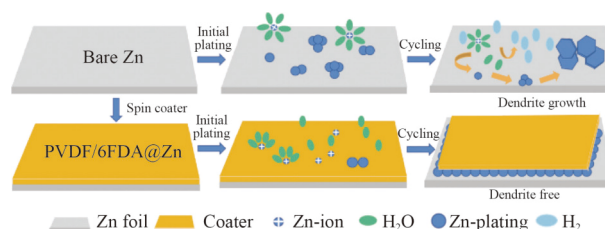


Fig. 1 Schematic diagram of the Zn deposition of bare Zn and PVDF/6FDA@Zn.

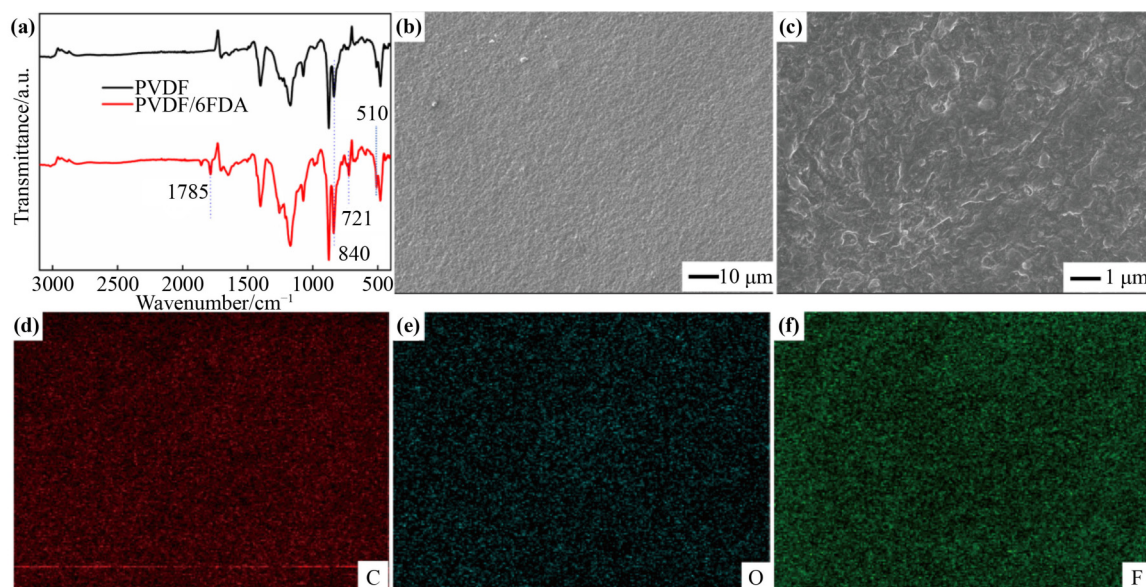


Fig. 2 (a) FTIR results of PVDF/6FDA and PVDF coatings. (b)(c) SEM images of the PVDF/6FDA coating. (d)(e)(f) C, O, and F elements distribution mapping images of the PVDF/6FDA coating.

successfully prepared. As shown in Fig. S2, a film with the thickness of 70 μm was curled to demonstrate the flexibility of the PVDF/6FDA film. The stress–strain curves of PVDF and PVDF/6FDA films with the same thickness are shown in Fig. S3. Compared to the PVDF coating, the PVDF/6FDA protective layer exhibits significantly improved flexibility with the elongation at break of 308.36%. In contrast, the elongation at break of PVDF is only 175.36%. Therefore, it can be deduced that PVDF/6FDA is more adaptable to the volume change caused by the zinc plating/stripping process.

To evaluate the hydrophilicity of the electrodes with ZnSO_4 , the contact angles of bare Zn, PVDF@Zn and PVDF/6FDA@Zn were measured at 25 $^\circ\text{C}$. As illustrated in Figs. 3(a) and 3(b), the initial contact angle of bare Zn is about 111.3 $^\circ$, which drops down to 108.9 $^\circ$ after 1 min. Figures 3(c) and 3(d) reveal that the contact angles of PVDF@Zn increase to 116.7 $^\circ$ and 115.4 $^\circ$, respectively. In contrast, the initial contact angle of PVDF/6FDA@Zn is only 85.2 $^\circ$, which gradually declines to 74 $^\circ$, suggesting that the addition of 6FDA enhances the hydrophilicity due to the presence of its anhydride groups. Meanwhile, as shown from EIS results (Fig. S4), the charge transfer resistance (R_{ct}) of the bare Zn symmetric cell is only 196 Ω , while R_{ct} values of bare Zn and PVDF@Zn are up to 347 and 328 Ω , respectively, indicating that the PVDF/6FDA film can accelerate the migration speed of Zn^{2+} and prevent the ingress of solvent water and anions. In addition, the ion conductivities of PVDF/6FDA films

with various thicknesses were measured, and the average ion conductivity was found to be 3.846 $\text{mS}\cdot\text{cm}^{-1}$ (Fig. S5). These results obtained are not significantly different from the findings reported in other studies.

It is significant that the anode maintains excellent electrochemical stability in neutral or slightly acidic aqueous electrolyte. Compared to bare Zn, PVDF/6FDA@Zn is likely to prevent side effects such as HER and the corrosion of basic zinc sulfate. The analysis on Tafel curves (Fig. S6) was conducted to determine the relationship between the anti-corrosion effect and the PVDF/6FDA coating. Unlike bare Zn, the corrosion potential of the coating changed from -0.974 to -0.966 V, and the corrosion current also reduced to 0.532 $\mu\text{A}\cdot\text{cm}^{-2}$. This means that the corrosion rate and the corrosion reaction probability of the coated electrode plunge.

In order to investigate the plating/stripping stability of the PVDF/6FDA@Zn electrode, the ultra-cyclic test of different symmetric cells has been performed at 0.5 $\text{mA}\cdot\text{cm}^{-2}$ (Figs. 4(a) and 4(b)). The deposition of the bare Zn symmetric cell encountered difficulty after cycling for nearly 260 h. The zinc foil with a PVDF layer can stabilize the cycling for 1000 h (Fig. S7). Encouragingly, the PVDF/6FDA coating can maintain the polarized voltage of 28 mV and the overpotential of only 8 mV under a stable cycle for 5000 h, which benefits from the effective inhibition on both the growth of zinc dendrites and the occurrence of side reactions. The PVDF/6FDA@Zn symmetric cell at the current density

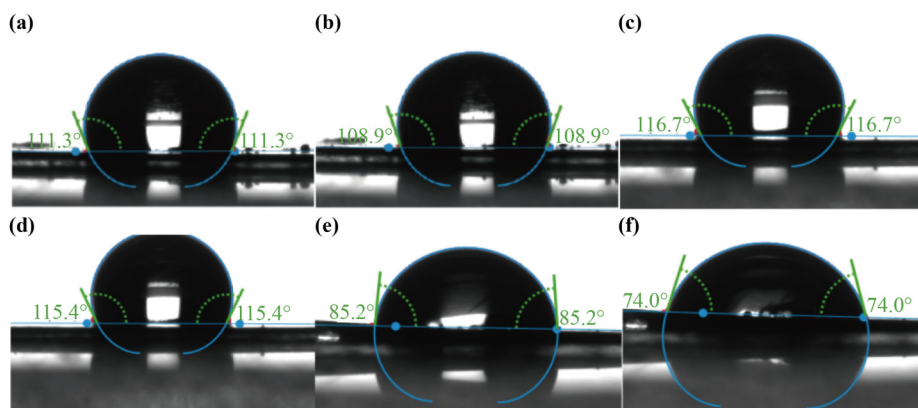


Fig. 3 Hydrophilicity results of Zn foils and coatings: (a)(b) contact angle measurements of bare Zn with $2 \text{ mol} \cdot \text{L}^{-1} \text{ ZnSO}_4$ at 0 and 1 min, respectively; (c)(d) results of PVDF@Zn, respectively; (e)(f) results of PVDF/6FDA@Zn, respectively.

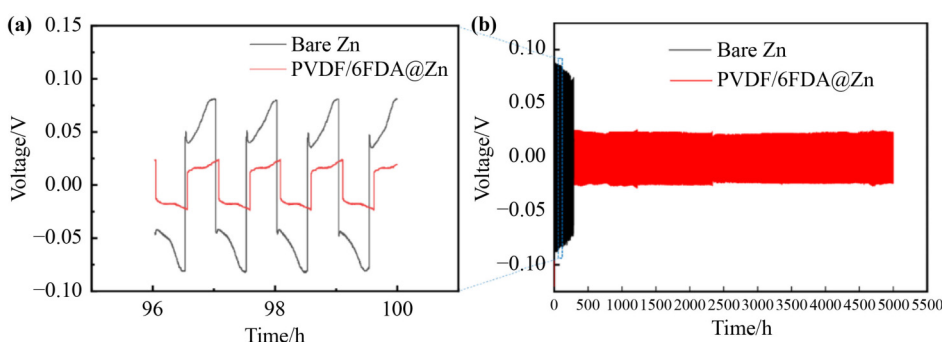


Fig. 4 (a) Partially enlarged comparative image of bare Zn and PVDF/6FDA@Zn symmetrical battery from the 96th to the 100th cycle. (b) Galvanostatic cycle test result of bare Zn and PVDF/6FDA@Zn symmetric cells at $0.5 \text{ mA} \cdot \text{cm}^{-2}$ and $0.25 \text{ mAh} \cdot \text{cm}^{-2}$.

ranging from 0.5 to $5 \text{ mA} \cdot \text{cm}^{-2}$ was also tested for rate stability (Fig. S8). It is detected that the electrode with coating continuously has a lower polarization voltage compared with that of bare Zn. From Table S1, it is seen that the cycle life values of most of previously published studies on modified zinc anodes are within 2000 h. Comparatively, the PVDF/6FDA@Zn symmetric cell in this study has an exceedingly longer cycle life than those summarized in this table.

The XRD results (Fig. S9) reveal the formation of basic zinc sulfate ($\text{Zn}_4\text{SO}_4(\text{OH})_6 \cdot x\text{H}_2\text{O}$) on the surface of the bare Zn anode as there are crystal planes of (1 0 1) and (1 0 0) representing sharp and vertically grown Zn, which can destroy the smooth and flat electrode, and more crystal planes of (0 0 2) representing the parallel zinc growth appearing on the surface of PVDF/6FDA@Zn. After 200 cycles at a current density of $0.5 \text{ mA} \cdot \text{cm}^{-2}$, SEM images of the bare zinc electrode are shown in Figs. 5(a)–5(c), from which some glass fiber films are observed on the surface of the zinc metal. Moreover,

irregular zinc deposits can also be observed, most of which are at a specific angle to the substrate. This arrangement is highly unfavorable for the stable circulation. The zinc deposition on the PVDF/6FDA-coated zinc foil is very uniform and dense, as shown in Figs. 5(d) and 5(e). The effect of the PVDF/6FDA protective layer on inhibiting the dendrite growth has been demonstrated, which also showcases the success of the surface modification strategy for zinc metal anodes.

As illustrated in Figs. 6(a) and S10, Zn||PVDF/6FDA@Cu can cycle steadily for more than 1200 h, more stable than bare Cu during the charge process. The cycle stability of the Zn||PVDF/6FDA@Cu half-cell is better than that of the Zn||Cu half-cell. This result is similar to that of the assembled symmetric cells, demonstrating that the PVDF/6FDA coating promotes the uniform deposition of zinc ions. In addition to achieving the uniform Zn deposition, the PVDF/6FDA layer can also enhance the reversibility of Zn plating/stripping and improve the coulombic efficiency (CE). As illustrated in Fig. 6(b), the

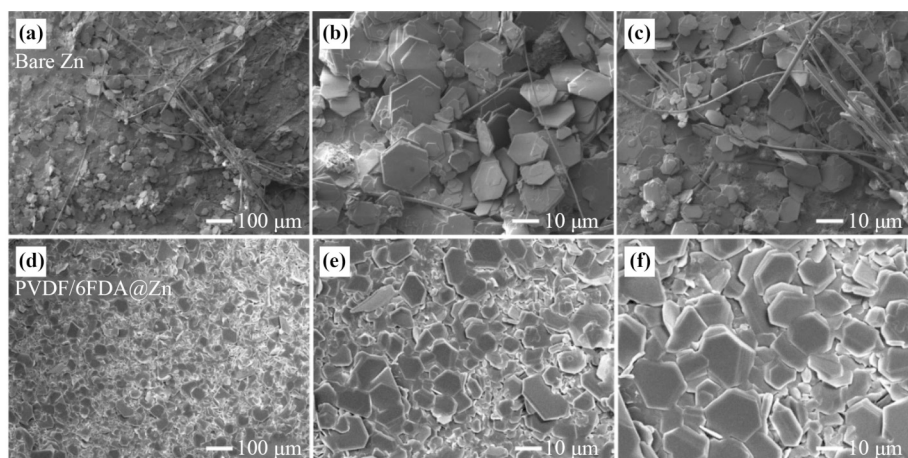


Fig. 5 SEM images of (a)(b)(c) the bare Zn electrode after 200 h cycle and (d)(e)(f) the PVDF/6FDA@Zn electrode after 200 h cycle.

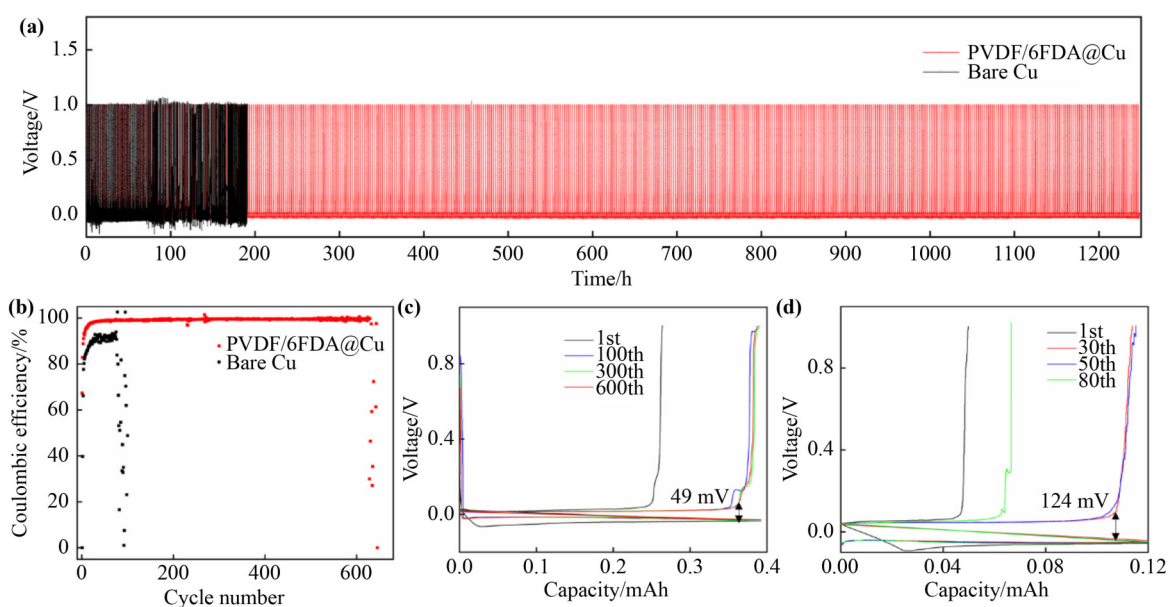


Fig. 6 (a) Cycle stability of Zn||Cu and Zn||PVDF/6FDA@Cu half-cells at 0.5 mA·cm⁻². (b) CE of plating/stripping of Zn||Cu and Zn||PVDF/6FDA@Cu half-cells at 0.5 mA·cm⁻². Voltage–capacity profiles of (c) the Zn||PVDF/6FDA@Cu half-cell and (d) the Zn||Cu half-cell.

Zn||PVDF/6FDA@Cu cell delivers a higher initial CE kept above 99% for 620 cycles. Moreover, the initial voltage hysteresis for the Zn||PVDF/6FDA@Cu half-cell is about 49 mV, much smaller than that of the bare Cu cell (124 mV) (Figs. 6(c) and 6(d)). These results suggest that PVDF/6FDA@Cu promote the formation of Zn²⁺ transport channels and the faster diffusion of zinc ions.

PVDF/6FDA@Zn||MnO₂ and Zn||MnO₂ full cells were assembled to prove the practical application capability of the PVDF/6FDA thin layer. The cells were charged/discharged in 2 mol·L⁻¹ ZnSO₄ + 0.2 mol·L⁻¹ MnSO₄

electrolyte. As shown in Fig. S11, at a current density of 0.1 C, the duration of one charging and discharging cycle for the entire battery is 58 h, and the cycle remains stable for up to 300 h.

The charging voltage of the cell was limited to 1.8 V while the discharging voltage was above 0.6 V. As shown in Fig. 7(a), MnO₂ presents typical redox peaks and reveals excellent reversibility from the current–voltage curve of the PVDF/6FDA@Zn||MnO₂ full cell. The rate performance ranging from 0.1 to 4 A·g⁻¹ of different full batteries was tested and presented in Fig. 7(b) to explain

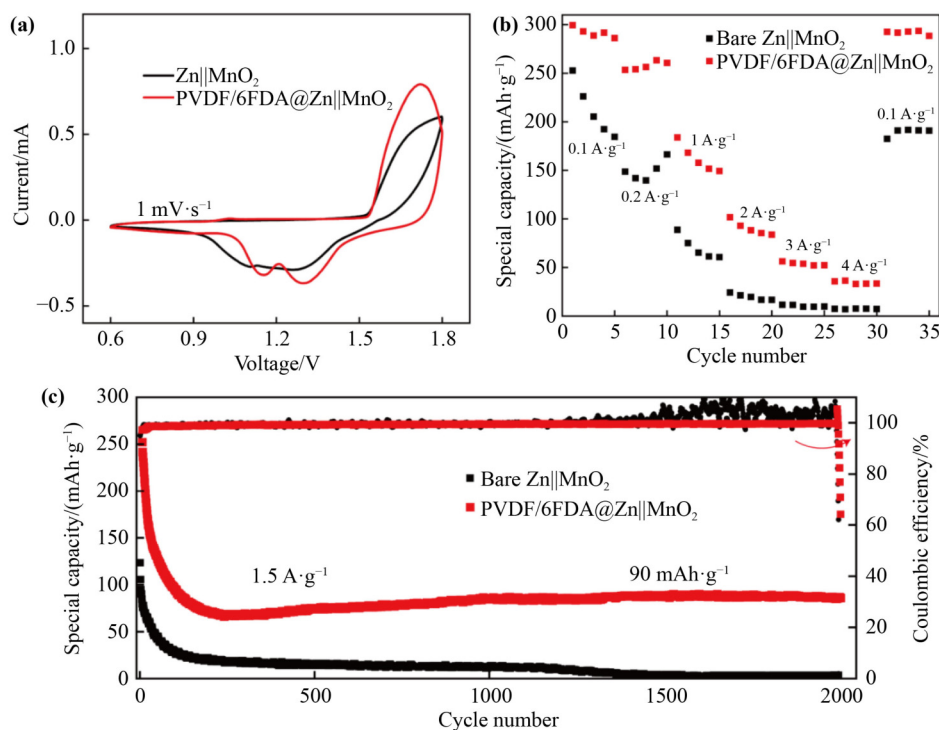


Fig. 7 Electrochemical test results of PVDF/6FDA@Zn||MnO₂ and Zn||MnO₂ full cells: (a) Current–voltage curves at the scanned rate of 1 mV·s⁻¹; (b) ratio performances from 0.1 to 4 A·g⁻¹ at MnO₂ mass; (c) long-cycling curves at 1.5 A·g⁻¹.

the influence of coating on specific capacity. The PVDF/6FDA@Zn||MnO₂ full cell exhibits high specific capacities of 286.1, 260.6, 149.3, 83.7, 52.3 and 33.5 mAh·g⁻¹ at current densities of 0.1, 0.2, 1, 2, 3 and 4 A·g⁻¹, respectively. Especially the specific capacity is 288.4 mAh·g⁻¹ when the current density is back to 0.1 A·g⁻¹, showing that the PVDF/6FDA film can effectively improve the migration of Zn²⁺ and slow down the specific capacity decay. Figure 7(c) shows the long cycle stability test of full cells conducted at 1.5 A·g⁻¹, in which the discharge specific capacity of the bare zinc anode indicates a rapid decay with the occurrence of serious deactivation after 1500 cycles. It is impressive that the PVDF/6FDA@Zn||MnO₂ full cell can maintain high discharge efficiency, cycle about 2000 times, and more importantly, keep the specific capacity at 90 mAh·g⁻¹ around. Consequently, it is revealed that PVDF/6FDA promote the Zn²⁺ migration and homogeneous compact deposition benefiting for specific capacity and rate performance.

4 Conclusion

In summary, the PVDF/6FDA coating has been prepared

by spin coating to protect Zn metal from the side reactions and the dendrite formation. Both PVDF and the organic compound 6FDA contain fluorine groups, which synergistically regulate the deposition/stripping of zinc ions. In addition, anhydride groups in 6FDA can improve the hydrophilicity of PVDF polymer coatings, reduce the interface impedance, and promote the zinc-ion transfer. Meanwhile, the PVDF/6FDA film with a low impedance can help the symmetric cell cycle stably for 5000 h at 0.5 mA·cm⁻² while the polarization voltage and the overpotential are 28 and 8 mV, respectively. The Zn||PVDF/6FDA@Cu cell also keeps a high CE above 99% after 620 cycles. It is impressive that the PVDF/6FDA@Zn||MnO₂ full cell achieve 2000 cycles at 1.5 A·g⁻¹ and the capacity keep stable at 90 mAh·g⁻¹ around. The zinc anode, assisted by a hydrophilic polymer coating, thus enables AZIBs to achieve high reversibility and long cycle life.

Declaration of competing interests The authors declare that they have no competing interests.

Acknowledgements This work was supported by the National Natural Science Foundation of China (Grant No. 51673154).

Electronic supplementary information Supplementary materials can be found in the online version at <https://doi.org/10.1007/s11706-023-0668-2> and <https://journal.hep.com.cn/foms/EN/10.1007/s11706-023-0668-2>, which include Figs. S1–S11 and Table S1.

References

- [1] Khalifa H, El-Safty S A, Reda A, et al. One-dimensional hierarchical anode/cathode materials engineering for high-performance lithium-ion batteries. *Energy Storage Materials*, 2021, 37: 363–377
- [2] Zeng Y, Chalise D, Lubner S D, et al. A review of thermal physics and management inside lithium-ion batteries for high energy density and fast charging. *Energy Storage Materials*, 2021, 41: 264–288
- [3] Chayambuka K, Mulder G, Danilov D L, et al. From Li-ion batteries toward Na-ion chemistries: challenges and opportunities. *Advanced Energy Materials*, 2020, 10(38): 2001310
- [4] Zhang X, Sun Q, Zhen C, et al. Recent progress in flame-retardant separators for safe lithium-ion batteries. *Energy Storage Materials*, 2021, 37: 628–647
- [5] Hosaka T, Kubota K, Hameed A S, et al. Research development on K-ion batteries. *Chemical Reviews*, 2020, 120(14): 6358–6466
- [6] Liu Y, Li L, Ji X, et al. Scientific challenges and improvement strategies of Zn-based anodes for aqueous Zn-ion batteries. *Chemical Record*, 2022, 22(10): e202200114
- [7] Wang F, Borodin O, Gao T, et al. Highly reversible zinc metal anode for aqueous batteries. *Nature Materials*, 2018, 17(6): 543–549
- [8] Glatz H, Tervoort E, Kundu D. Unveiling critical insight into the Zn metal anode cyclability in mildly acidic aqueous electrolytes: implications for aqueous zinc batteries. *ACS Applied Materials & Interfaces*, 2020, 12(3): 3522–3530
- [9] Jia H, Wang Z, Tawiah B, et al. Recent advances in zinc anodes for high-performance aqueous Zn-ion batteries. *Nano Energy*, 2020, 70: 104523
- [10] Shang Y, Kundu D. Understanding and performance of the zinc anode cycling in aqueous zinc-ion batteries and a roadmap for the future. *Batteries & Supercaps*, 2022, 5(5): e202100394
- [11] Yang Z, Lv C, Li W, et al. Revealing the two-dimensional surface diffusion mechanism for zinc dendrite formation on zinc anode. *Small*, 2022, 18(43): 2104148
- [12] Yang Q, Li Q, Liu Z, et al. Dendrites in Zn-based batteries. *Advanced Materials*, 2020, 32(48): 2001854
- [13] Yang J, Zhao R, Wang Y, et al. Insights on artificial interphases of Zn and electrolyte: protection mechanisms, constructing techniques, applicability, and prospective. *Advanced Functional Materials*, 2023, 33(14): 2213510
- [14] Hu Y, Li Z, Wang Z, et al. Suppressing local dendrite hotspots via current density redistribution using a superlithiophilic membrane for stable lithium metal anode. *Advanced Science*, 2023, 10(12): 2206995
- [15] Li D, Wei Z, Lei W, et al. *In situ* crosslinked hybrid aluminum polymer film for high-performance solid electrolyte interphase of lithium metal battery. *Journal of Power Sources*, 2023, 563: 232808
- [16] Wang X, Sun C, Wu Z S. Recent progress of dendrite-free stable zinc anodes for advanced zinc-based rechargeable batteries: fundamentals, challenges, and perspectives. *SusMat*, 2023, 3(2): 180–206
- [17] Zhou L F, Du T, Li J Y, et al. A strategy for anode modification for future zinc-based battery application. *Materials Horizons*, 2022, 9(11): 2722–2751
- [18] Nie W, Cheng H, Sun Q, et al. Design strategies toward high-performance Zn metal anode. *Small Methods*, 2023, 7: 2201572
- [19] Ren Q, Tang X, Zhao X, et al. A zincophilic interface coating for the suppression of dendrite growth in zinc anodes. *Nano Energy*, 2023, 109: 108306
- [20] Guo W, Cong Z, Guo Z, et al. Dendrite-free Zn anode with dual channel 3D porous frameworks for rechargeable Zn batteries. *Energy Storage Materials*, 2020, 30: 104–112
- [21] Chladil L, Cech O, Smejkal J, et al. Study of zinc deposited in the presence of organic additives for zinc-based secondary batteries. *Journal of Energy Storage*, 2019, 21: 295–300
- [22] Mitha A, Mi H, Dong W, et al. Thixotropic gel electrolyte containing poly (ethylene glycol) with high zinc ion concentration for the secondary aqueous Zn/LiMn₂O₄ battery. *Journal of Electroanalytical Chemistry*, 2019, 836: 1–6
- [23] Yang X, Liu S, Tang J, et al. Effective inhibition of zinc dendrites during electrodeposition using thiourea derivatives as additives. *Journal of Materials Science*, 2019, 54(4): 3536–3546
- [24] Naveed A, Yang H, Yang J, et al. Highly reversible and rechargeable safe Zn batteries based on a triethyl phosphate electrolyte. *Angewandte Chemie International Edition*, 2019, 58(9): 2760–2764
- [25] Wang F, Borodin O, Gao T, et al. Highly reversible zinc metal anode for aqueous batteries. *Nature Materials*, 2018, 17(6): 543–549
- [26] Zhao Z, Zhao J, Hu Z, et al. Long-life and deeply rechargeable aqueous Zn anodes enabled by a multifunctional brightener-inspired interphase. *Energy & Environmental Science*, 2019, 12(6): 1938–1949
- [27] Zhao J, Zhang J, Yang W, et al. “Water-in-deep eutectic solvent” electrolytes enable zinc metal anodes for rechargeable aqueous batteries. *Nano Energy*, 2019, 57: 625–634
- [28] Chen P, Yuan X, Xia Y, et al. An artificial polyacrylonitrile coating layer confining zinc dendrite growth for highly reversible aqueous zinc-based batteries. *Advanced Science*, 2021, 8(11): 2100309

- [29] Zeng X, Xie K, Liu S, et al. Bio-inspired design of an *in situ* multifunctional polymeric solid–electrolyte interphase for Zn metal anode cycling at $30 \text{ mA}\cdot\text{cm}^{-2}$ and $30 \text{ mAh}\cdot\text{cm}^{-2}$. *Energy & Environmental Science*, 2021, 14(11): 5947–5957
- [30] Niu B, Li Z, Cai S, et al. Robust Zn anode enabled by a hydrophilic adhesive coating for long-life zinc-ion hybrid supercapacitors. *Chemical Engineering Journal*, 2022, 442: 136217
- [31] Hieu L T, So S, Kim I T, et al. Zn anode with flexible β -PVDF coating for aqueous Zn-ion batteries with long cycle life. *Chemical Engineering Journal*, 2021, 411: 128584
- [32] Wang X, Wang X, Zhou Y, et al. *In-situ* construction of multifunctional protection interface for ultra-stable zinc anodes. *Journal of Alloys and Compounds*, 2023, 947: 169510
- [33] Wei T, Zhang X, Ren Y, et al. Reconstructing anode/electrolyte interface and solvation structure towards high stable zinc anode. *Chemical Engineering Journal*, 2023, 457: 141272
- [34] Tao F, Feng K, Liu Y, et al. Suppressing interfacial side reactions of zinc metal anode via isolation effect toward high-performance aqueous zinc-ion batteries. *Nano Research*, 2023, 16(5): 6789–6797
- [35] Hao J, Li X, Zhang S, et al. Designing dendrite-free zinc anodes for advanced aqueous zinc batteries. *Advanced Functional Materials*, 2020, 30(30): 2001263
- [36] Ge X, Zhang W, Song F, et al. Single-ion-functionalized nanocellulose membranes enable lean-electrolyte and deeply cycled aqueous zinc-metal batteries. *Advanced Functional Materials*, 2022, 32(26): 2200429
- [37] Zhang Z, Wang R, Hu J, et al. An *in situ* self-assembled 3D zincophilic heterogeneous metal layer on a zinc metal surface for dendrite-free aqueous zinc-ion batteries. *Sustainable Energy & Fuels*, 2021, 5(22): 5843–5850
- [38] Xie C, Li Y, Wang Q, et al. Issues and solutions toward zinc anode in aqueous zinc-ion batteries: a mini review. *Carbon Energy*, 2020, 2(4): 540–560
- [39] Lee S, Song G, Kim S, et al. Ion-selective and chemical-protective elastic block copolymer interphase for durable zinc metal anode. *Cell Reports Physical Science*, 2022, 3(10): 101070
- [40] Zhao R, Yang J, Han X, et al. Stabilizing Zn metal anodes via cation/anion regulation toward high energy density Zn-ion batteries. *Advanced Energy Materials*, 2023, 13(8): 2203542